*Journal of Engineering Research and Reports*

***Volume 24, Issue 1, Page 30-48, 2023; Article no.JERR.94359***
***ISSN: 2582-2926***

# Application of ANN and RSM Techniques in Optimal Parameter Evaluation for Turbidity Removal from Abattoir Effluent using Valorized Chicken Bone Coagulant

**Frankly Chukwudi Chime [a], Paschal Enyinnaya Ohale [a*], Chijioke Elijah Onu [a*] and Nonye Jennifer Ohale [a]**

*[a] Department of Chemical Engineering, Nnamdi Azikiwe University Awka, Anambra state, Nigeria.*

***Authors' contributions***

*This work was carried out in collaboration among all authors. All authors read and approved the final manuscript.*

***Article Information***

DOI: 10.9734/JERR/2023/v24i1795

**Open Peer Review History:**
This journal follows the Advanced Open Peer Review policy. Identity of the Reviewers, Editor(s) and additional Reviewers, peer review comments, different versions of the manuscript, comments of the editors, etc are available here: https://www.sdiarticle5.com/review-history/94359

***Original Research Article***

***Received: 21/10/2022***
***Accepted: 23/12/2022***
***Published: 13/01/2023***

## ABSTRACT

Chicken bone coagulant (CBC) containing high grade hydroxyapatite (HPA) has been applied in the coag-flocculation of abattoir effluent. The influence of process variables (pH, initial concentration, dosage, Temperature, and settling time) on the effluent final turbidity was investigated. Also, the accuracies of two modelling techniques (Response surface methodology, RSM and Artificial neutral network, ANN) in predicting the non-linear nature of the system were compared. The optimization result indicates a final turbidity of 4.96 mg/L (corresponding to 98.28 % removal efficiency) at pH = 6.7, dosage = 1.003 g/L, initial conc. = 182.2 mg/L, coagulation temp. = 345 K and settling time of 36 min. Meanwhile, effluent pH was spotted as the most significant

**Corresponding author: E-mail: pe.ohale@unizik.edu.ng, ce.onu@unizik.edu.ng;*

variable, with p-value <0.01%. Furthermore, the error analysis result portrayed the supremacy of ANN over RSM in data prediction accuracy as it signified lower error values (Mean square error, MSE = 13.11 and Absolute average relative deviation, AARD = 1.43%) when compared to those of RSM (MSE = 37.78, AARD = 5.93%). Thus, it was demonstrated that ANN is a better tool for optimization study of the present system.

*Keywords: Abattoir-effluent; turbidity; hydroxyapatite; chicken bone; artificial neural network.*

## 1. INTRODUCTION

One of the most essential ingredients for human existence and the sustaining of life as a whole is fresh water. Even though there is an increased need for fresh water due to population expansion and increasing urbanization [1]. The greatest problem for those who use fresh water resources is still pollution, which also jeopardizes the survival of natural habitats. The release of dangerous pollutants into already stressed fresh water bodies, so contaminating them, exacerbates the difficulty of assuring the supply of fresh water for the teeming populace.

The operations of the slaughterhouse sector continue to be a significant cause of environmental contamination while also serving as a key way of supplying Nigeria's enormous population with protein. Approximately 6% of the nation's total GDP and 20% of the agricultural GDP are contributed by the sector [2, 3] (Ohale et al., [4]. Animals are slaughtered, washed, butchered, and then packaged in raw form for further treatment or consumption as part of the fundamental meat production procedures carried out in an abattoir. These operations produce a significant amount of wastewater, often known as abattoir-effluent Various organic contaminants from the paunch, excrement, fat and lard, grease, unprocessed food, blood, dispersed matter, urine, soluble proteins, manure, grit, condemned meat, and colloidal particles are frequently present in slaughterhouse wastewater. Abattoir wastewater is characterized by its foul odor, black color, and low bacteriological quality, all of which are caused by these pollutants [5] Ohale et al., [4]. The deterioration of the groundwater and contamination of waterways and irrigation water with excessive organic matter are both considerably exacerbated by the discharge of slaughter house wastewater into the environment without proper treatment [5, 6].

In experimental and pilot size investigations, several studies have satisfactorily used a variety of methodologies for the remediation of slaughterhouse wastewater. Some of the investigated treatment procedures include electro-coagulation, electro-sequencing, ventilated lagoon systems, high rate algal reservoirs, halophyte therapy, and integrated bio treatment systems [7, 8, 5,4]. Some of the investigated treatment procedures include electro-coagulation, electro-sequencing, ventilated lagoon systems, high rate algal reservoirs, halophyte therapy, and integrated bio treatment systems. The significant energy requirement for ventilation, creation of surplus sludge, time-consuming processing rate brought on by buildup of suspended solids, and floating fats in the reactor, unfortunately, limit the effectiveness of anaerobic treatment options [9, 10]. Many studies still choose to use coagulation and flocculation to control highly turbid pollutants due to the constraints of anaerobic treatment methods [9, 11]. This can be as a result of their operational cost efficiency and flexibility. In order for the large floccus to settle and be separated by decantation, the coagulation and flocculation process must generate large floccus which are heavier than the carrier wastewater. Three distinct and consecutive processes make up the complete coagulation process: coagulant production, particle instability, and inter-particle interactions [12, 11, 5]. Coagulant dose, coagulation temperature, effluent pH, and effluent concentration are the key coagulation process variables. Al-Mutairi et al [13], and Amuda & Alade [14] examined the use of poly-aluminum chloride and aluminum salt as effective coagulants for the treatment of abattoir wastewater. Aquilar, et al., [15], reported that treating abattoir wastewater with alum alone has a highest turbidity reduction effectiveness of 87%. Furthermore, Amudaa & Alade, [14] achieved a substantial reduction in COD from abattoir effluent using 1000 mg/L of alum. Mahtaba, et al., [16] reported 99 % removal of suspended solids by using 400 mg/L of alum and 30 mg/L of polymer. However, it has been noted that using these synthetic coagulants have adverse health consequences. According to Katayon et al. [17], several negative effects linked with the application of chemical coagulants include Alzheimer's disease, excess sludge production, cost inefficiency, and the introduction of significant changes in chemical characteristics

of water resulting from reactions with the OH- and basicity of water. Therefore, using bio-coagulants will potentially greatly reduce the regular issues associated with the usage of metal salts and synthetic coagulants [17].

Several scientists have developed a range of organic coagulants for the treatment of severely turbid waste water. Some of which are crab-shell chitin (Saritha, et al., 2015), snail shell extract [12], Dromedary bone [18], Periwinkle shell [12]. Recently, scientists' attention has been devoted to the use of animal bones for the treatment of different forms of wastewater [19, 20]. Studies have shown that animal bones contain an active ingredient called hydroxyapatite (HAP), which has been proven to be very useful in surface driven wastewater treatment processes such as coagulation [18,20]. Hydroxyapatite (HAP) has a highly stable calcium phosphate hexagonal structure which can withstand extreme conditions of temperature and pH. Many researchers have successfully used HAP in removal of heavy metals [21, 20], turbidity [19], and dye wastewater [18]. Therefore, our present study is essential in order to further give a remedy to the environmental degradation caused by the potential for inappropriate release of slaughterhouse effluents. The study examines the production of chicken bone (CB) coagulant and its possible application in the coag-flocculation treatment of abattoir-effluent. Although the effectiveness of numerous natural coagulants in the treatment of abattoir effluent via coag-flocculation process have been widely reported in literature, however, to the best of our knowledge, there has not been any reported use of chicken bone coagulant (CBC) in the treatment of abattoir-effluent.

Previously, “one-factor at a time” (OFAT) was the strategy that most researchers used to determine the best experimental parameters. However, the OFAT method is typically time- and labor-intensive. Also, It rarely provides the desirable optimum that is sought after. Utilizing empirical design methodological approaches, these limitations related to the usage of the OFAT technique can be overcome. RSM and ANN have lately been combined as an empirical design optimization algorithm in wastewater treatment research [22, 23, 24; 25, 26]. RSM is employed in industrial processes to either produce high-quality items or run a process more efficiently [27, 28]. RSM's primary goal is to use experimental methods to optimize an uncertain and noisy parameter using simpler approximate functions that are viable over a constrained region. Numerous studies have reported using the RSM method to successfully optimize process variables [29, 30]. Additionally, as a result of the transdisciplinary expansion of modern analytical approaches, artificial neural networks (ANNs), which are common artificial intelligence (AI) algorithms, have emerged as a contemplated method for modeling resilient and non-linear systems (Ohale et al., 2022a). The capability of ANN to learn from previous events and its general structure are its key characteristics. It is often believed that ANN could require much more number of experiments than RSM to build an efficient model [31]. However, research has shown that a comparatively smaller amount of data can still be utilized if it is statistically properly distributed throughout the input vector (Shafi et al., 2018; Onu et al., [32]). Also, the experimental data of any well-defined RSM would be sufficient to build an effective ANN model. Literature studies have shown that ANN model consistently worked better than RSM model in predicting the response of non-linear systems [33, 34].

This study therefore intends to critically analyze and derive a model for final turbidity reduction of abattoir-effluent using the most significant process factors. The accuracy of ANN and RSM techniques in modelling the coag-flocculation process will be comparatively assessed. Also, the formulated objective function would be optimized using hybrid ANN-Genetic algorithm (ANN-GA) technique.

## 2. MATERIALS AND METHODS

### 2.1 Materials

The abattoir effluent was collected from a local slaughterhouse located at Amasea in Anambra state, Nigeria. Chicken bones were collected from refuse were collected from fast food waste around Awka, in Anambra state, Nigeria. Furthermore, analytical grade chemical reagents utilized in the experiment were obtained from the Chemical Engineering Laboratory of Nnamdi Azikiwe University, Awka, Nigeria.

### 2.2 Sample Pre-Treatment and Storage

The collected abattoir-effluent was preserved by refrigeration. Prior to each stage of treatment, the effluent was allowed to sediment for 24 h and afterwards decanted. Sediments which are majorly composed of very fine particles which

could not undergo gravity settling were afterwards stored (in refrigerator) for coag-flocculation treatment. The chicken bones (CB) were washed with deionized water to remove the marrow and inherent dirt, afterwards they were cut into fragments of 2–5 g mass, boiled in distilled water and dried at a temperature of 90 $^0$C for 8 h onto constant weight.

## 2.3 Extraction of Active Coagulant

The procedure reported by Brezinska-Miecznik et al., [35] was adopted in the extraction of hydroxyapatite (HPA) from chicken bones (CB). Briefly, the dried CB fragments were treated with 4M NaOH solution at 90 $^o$C for 12 days. The sample to solution ratio of the treatment was kept 1 g of sample to 90 cm$^3$ of solution. At the end of the treatment procedure, the treated samples were repeatedly washed with distilled water until the pH of the filtrate approached neutrality. The washed samples were dried at 150 $^o$C for 10 h, after which they were crushed using mechanized crusher to particle size of 70 µm (using a Particle Size Distribution Analyzer - Model 117.08, MALVERN Instruments, USA) and then stored in an air tight container.

## 2.4 Abattoir-Effluent Sample Calibration and Characterization

In order to establish a logical link between the units of turbidity (NTU) and those of concentration (mg/L), serial dilution of the raw effluent was obtained. For each of the dilute solutions, characteristic concentration in NTU and the corresponding amount (mg) per volume of the sample were obtained using turbidity meter (Hanna Instruments, Model: LP2000) and sensitive weighing balance (JA-SARIES, Model: JA203H), respectively. Results obtained from the effluent calibration were supplied in section 3.1. Furthermore, American Public Health Association (APHA) standard procedure as reported by Clesceri, *et al.,* [36] was adopted for the physicochemical characterization of the abattoir-effluent. Elaborate discussion of findings from the physicochemical characterization of the effluent was presented in section 3.2.

## 2.5 Coagulant Characterization

The physicochemical properties and degree of effectiveness of the chicken bone coagulant (CBC) extraction process was ascertained by characterization. The structural vibration, topographical stabilization, and the crystallinity of the CB and CBC were determined using Fourier Transform Infra-red Spectroscopy (FTIR) (ThermoNicolet Nexus Model 470/670/870), Scanning Electron Microscopy (SEM) (Model Zeiss Evo®MA 17 EDX/WDS microscope), and X-ray Diffraction (XRD) (PHILIPS X PERT X – RAY diffraction unit with Cu Kr radiation), respectively. All the instrumental analysis was carried out according to ASTM E1508 and ASTM E168 standards.

## 2.6 Jar Test Procedure and Experimental Design

The jar test procedure was carried out based on standard Bench scale nephelometric technique for investigation of water and waste water (AWWA, 2005 and WST, 2003), using Model LP-2000 Hanna Instruments Turbidimeter, Search tech Instruments 78 HW-1 magnetic stirrer and PHS-3C 005399 pH meter.

The pH of the effluent was adjusted to pH 3, 4, 6, 8 and 10 using 1 M $H_2SO_4$ and 1 M NaOH, after which appropriate amounts (0.7, 1.0, 1.6, 2.2, and 2.5 g/L) of CBC were added to each 500 ml beaker containing different concentrations of abattoir effluent (100, 184, 350, 517, 600 mg/L) as illustrated in Table 2.

Central Composite Design (CCD) was applied in this work to model the coagulation process of turbidity removal from abattoir effluent. The design consists of a 2n factorial or fraction (coded to the usual ±1 notation) augmented by 2n axial points (±α, 0, 0,..., 0), (0, ±α, 0,..., 0),..., (0, 0,..., ±α), and $n_c$ centre points (0, 0, 0,..., 0). The statistical relevance of each parameter was evaluated using analysis of variance (ANOVA) (Ohale, *et al.,* 2017). If all variables are assumed to be measurable, the response surface can be expressed as Eq. (1). RSM optimizes the response variable (y) and searches for a suitable approximation of the functional relationship between the independent variables and the response surface.

$$y = b_0 + \sum b_i X_i + \sum b_{ii} X_{ii}^2 + \sum b_{ij} X_i X_j + \varepsilon \quad (1)$$

For statistical analysis, the experimental variable $X_i$ has been coded as $x_i$ as shown in Eq. 2:

$$x_i = \frac{X_i - X_n}{\Delta X_i} \quad (2)$$

Where $x_i$ is the coded value (dimensionless) of the $ith$ independent variable, $X_i$ is the un-coded value of the $ith$ independent variable, $X_n$ is the real value of an independent variable at the centre point and $\Delta X_i$ is the step change value of the real variable *i*. The relationship between the coded value and level of variance is presented in Table 1.

Where; $X_{min}$ and $X_{max}$ are minimum and maximum values of X, respectively. Applying the relationships in Table 1, the values of the codes were calculated and shown in Table 2.

The experimental plan was generated using the Design-Expert program 11.0 trial version (Stat-Ease Inc., Minneapolis, USA).

### 2.7 Artificial Neural Network (ANN)

The creation of ANN utilized the Multi Layer Perceptron (MLP) with the Marquardt Levenberg method employing back propagation algorithm. The MLP was performed in MATLAB (The mathworks, inc., 2009 b), having five input variables comprising the input layer, and the ultimate turbidity being the sole output neuron. The biases and the total of a neuron's weighted inputs make up the input weights. The neuron is described by the mathematical statement in Eq. (3).

$$Y_i = \sum_{i=1}^{n} x_i \omega_i + \theta_i \tag{3}$$

Where; $Y_i$ is the net input to the node, *i* in the hidden layer, $w_i (i = 1, n)$ are the connection weights, $\theta_i$ is the bias and $x_i$ is the input parameter. The weighted output was passed through a nonlinear activation process by applying the logistic output function given in Eq. (4);

$$f(sum) = \frac{1}{1 + \exp(-sum)} \tag{4}$$

The artificial neural network's structural framework utilized in this study is described in Fig. 1. Fig. 1 shows that the output from the input layer formed an input for the hidden layer. Similarly, the output layer receives an input from the hidden layer.

A acceptable number was determined via predictive and error function testing, with the concealed number of neurons randomly ranging from 2 to 11 (see Eqs. 5 & 6, respectively) on the outputs obtained (by varying the number of neurons). The tests compare the deviation of their predictions from the experimental values [37].

$$R^2 = 1 - \frac{\sum_{i=1}^{i=n} \left( y_{i,predic} - y_{i,\exp} \right)^2}{\sum_{i=1}^{i=n} \left( y_{i,\exp} - y_{av} \right)^2} \tag{5}$$

$$RMSE = \sqrt{\frac{\sum_{i=n}^{n} \left( y_{i,predic} - y_{i,\exp} \right)^2}{n}} \tag{6}$$

Where n is the number of data points, $y_{i,predic}$ is the network prediction at a specific number of hidden neurons, $y_{i,\exp}$ is the real experimental response, $y_{av}$ is mean value of experimental data and *i* is the data index.

## 3. RESULT AND DISCUSSIONS

### 3.1 Calibration of Abattoir Effluent

The result of effluent calibration was presented in Fig. 2. Fig. 2 shows the existence of a direct proportional relationship between the amount of particles (mg) and the turbidity (NTU). Linear correlation models given in Eqs. (7) and (8) were obtained from the calibration analysis and were subsequently utilized in converting the concentration of abattoir effluent from NTU to mg/L.

$$C_{mg/L} = 1.841 C_{NTU} - 11.368 \tag{7}$$

$$C_{mg/L} = 1.81 C_{NTU} \tag{8}$$

Where; $C_{mg/L}$ and $C_{NTU}$ are the effluent concentrations in mg/L and NTU, respectively. Eq. (8) strictly applies to abattoir effluent with very low concentrations (NTU < 6.18), while Eq. (7) applies to abattoir effluents with turbidity concentration higher than 6.18.

**Table 1. Relationship between coded value and the level of variance**

| Coded value | Level of variance |
|---|---|
| -α | $X_{min}$ |
| -1 | $[(X_{min} + X_{max})/2] – [(X_{max} – X_{min}) / 2b]$ |
| 0 | $[(X_{min} + X_{max})/2]$ |
| +1 | $[(X_{min} + X_{max})/2] + [(X_{max} – X_{min}) / 2b]$ |
| + α | $X_{max}$ |

**Table 2. Levels of independent variables for CCD experimental design**

| Independent variables | | Symbol | Coded variable levels | | | | |
|---|---|---|---|---|---|---|---|
| | | | -α | -1 | 0 | +1 | +α |
| pH | | $X_1$ | 3 | 4 | 6 | 8 | 9 |
| Dosage | g/L | $X_2$ | 0.7 | 1.0 | 1.6 | 2.2 | 2.5 |
| Initial conc. | mg/L | $X_3$ | 100 | 184 | 350 | 517 | 600 |
| Temperature | K | $X_4$ | 301 | 310 | 327.5 | 345 | 354 |
| Settling time | min | $X_5$ | 6.3 | 15 | 32 | 50 | 59 |

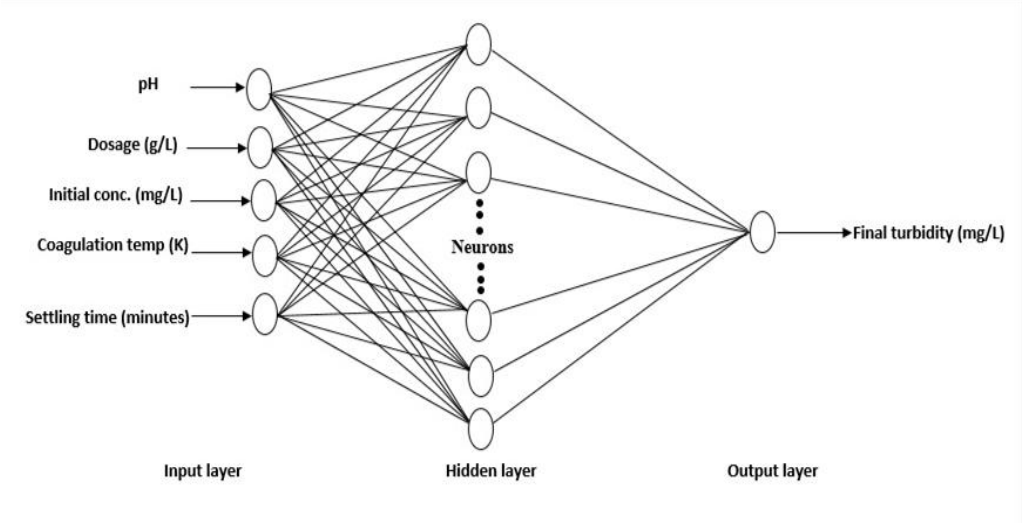


**Fig. 1. Architecture of the developed artificial neural network**

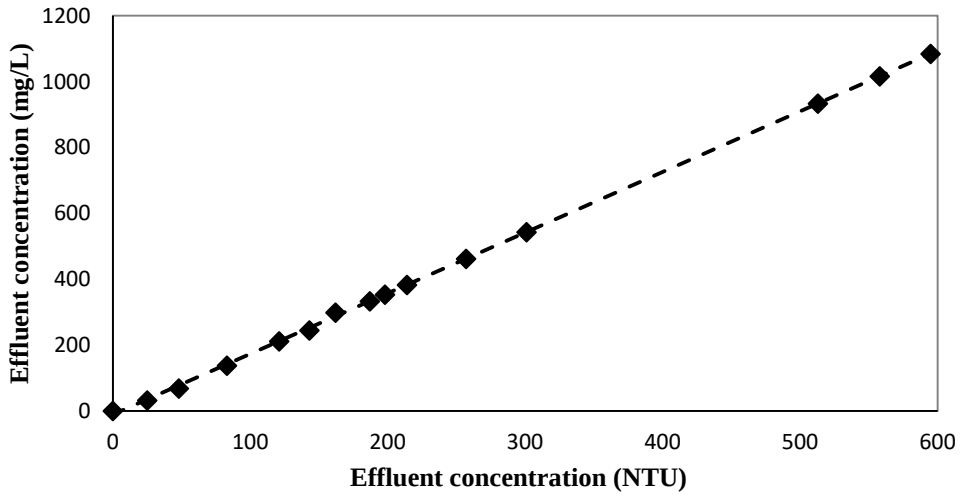


**Fig. 2. Abattoir-effluent calibration plot**

**Table 3. Physicochemical characteristics of abattoir-effluent**

| Parameters | Concentration | FEPA |
|---|---|---|
| Initial turbidity concentration (mg/L) | 599 | <100 |
| Total suspended solids (mg/L) | 1030.8 | <100 |
| Total solids (mg/L) | 1614.8 | <500 |
| Biological oxygen demand $(mg/L)_5$ | 220 | 210 |
| Chemical oxygen demand (mg/L) | 692 | <180 |
| pH | 7.5 | 6 – 9 |
| Odour | Objectionable | Odorless |
| Colour | Dark red | - |

## 3.2 Waste Water Characteristics

The physicochemical characteristics of the raw effluent prior to treatment is presented in Table 3. A close observation of Table 3 shows that only the effluent pH is within the permissible discharge limit as stipulated by the Environmental Protection Act (EPA). The total suspended solids (TSS) and the total solids (TS) which bear major influence on the effluent turbidity, were significantly higher than the tolerable EPA threshold for effluent discharge; thus justifying the need for treatment.

## 3.3 Instrumental Characterization of the CSC

### 3.3.1 FTIR spectra analyses

The FTIR spectra of CB and CBC are shown in Figs. 3 (a) and 4 (b), respectively. Visual inspection of the spectra results show that the obtained CBC spectra fall within the frequency of 3325 – 650 $cm^{-1}$. According to Coutts [38], the observation peaks below 600 $cm^{-1}$ are not applicable for characterizing wavebands. The vibrational peak at 663.5 $cm^{-1}$ which is attributed to OH functional group, became more conspicuous in CBC following NaOH treatment. The absorption intensity at 1241.2 $cm^{-1}$ in the raw CB shifted to 1244.9 $cm^{-1}$ after the HAP extraction process. This waveband (1241.2 $cm^{-1}$) demonstrates the presence of $CO_3^{2-}$ which indicates a major characteristic property of HAP. The peak at 1032.5 $cm^{-1}$ indicates the presence of C–O bending of the glucose molecule due to C–O–C linkage. The presence of phosphorus compound (P–F stretching) is displayed on 898.3 $cm^{-1}$, while its presence in the CBC (HPA) spectra shows the presence of N – H wagging band of the protein compounds. The C–O stretching band at 1159.2 $cm^{-1}$ indicates the presence of anhydrides in the CBC; while those at 3324.8 $cm^{-1}$ suggest the presence of N – H amides (Brzezińska-Miecznik et al., 2014).

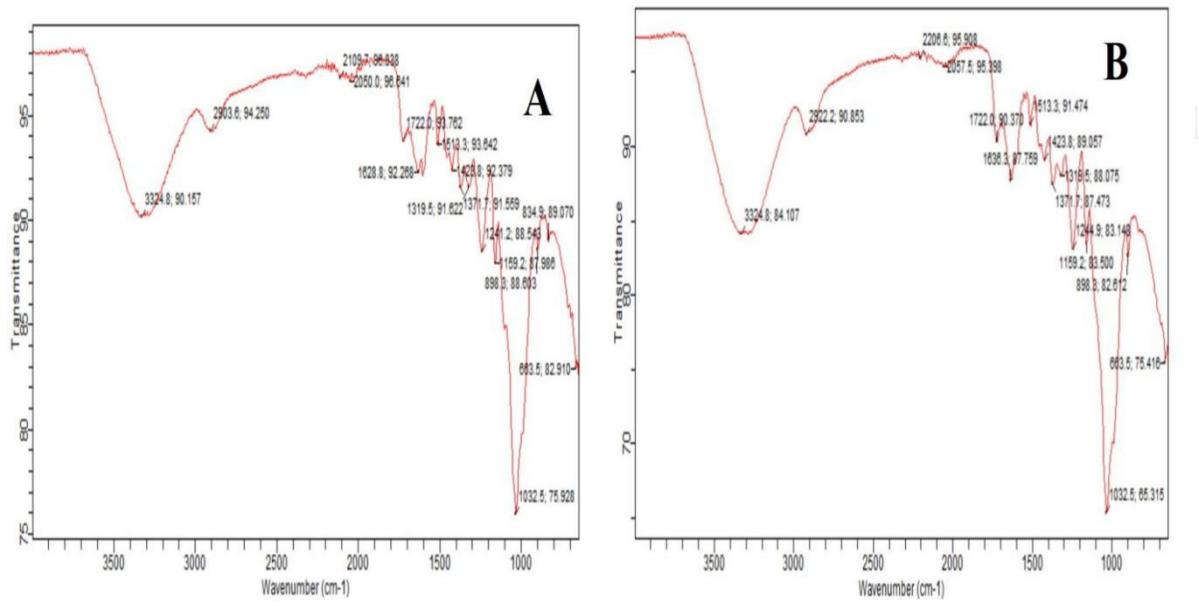


**Fig. 3. FTIR spectra of (a) CB (b) CBC**

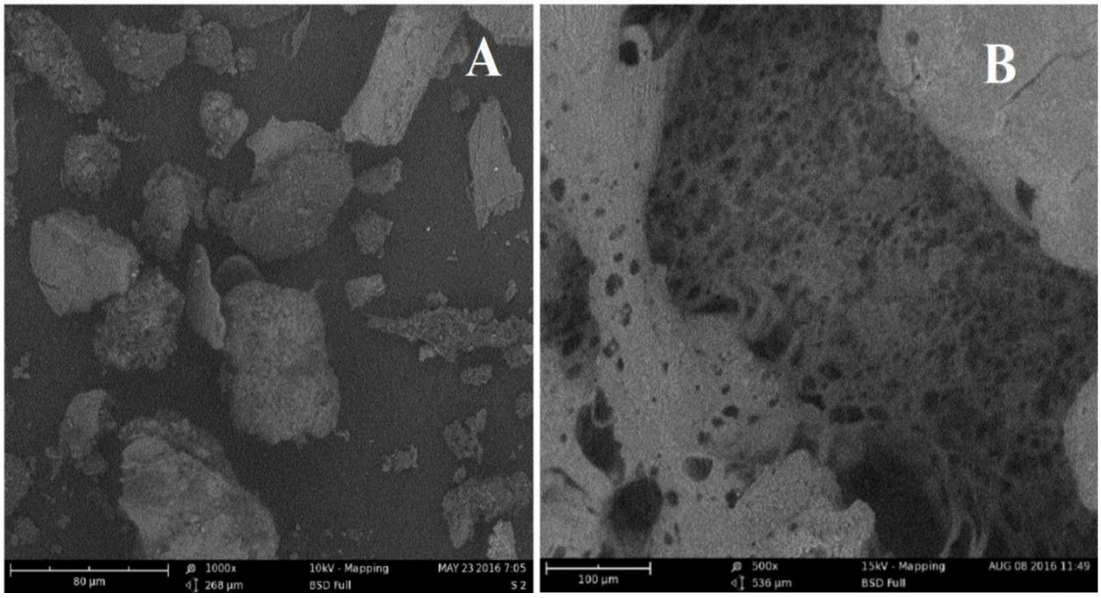


**Fig. 4. SEM micrograph of (a) CB (b) CBC**

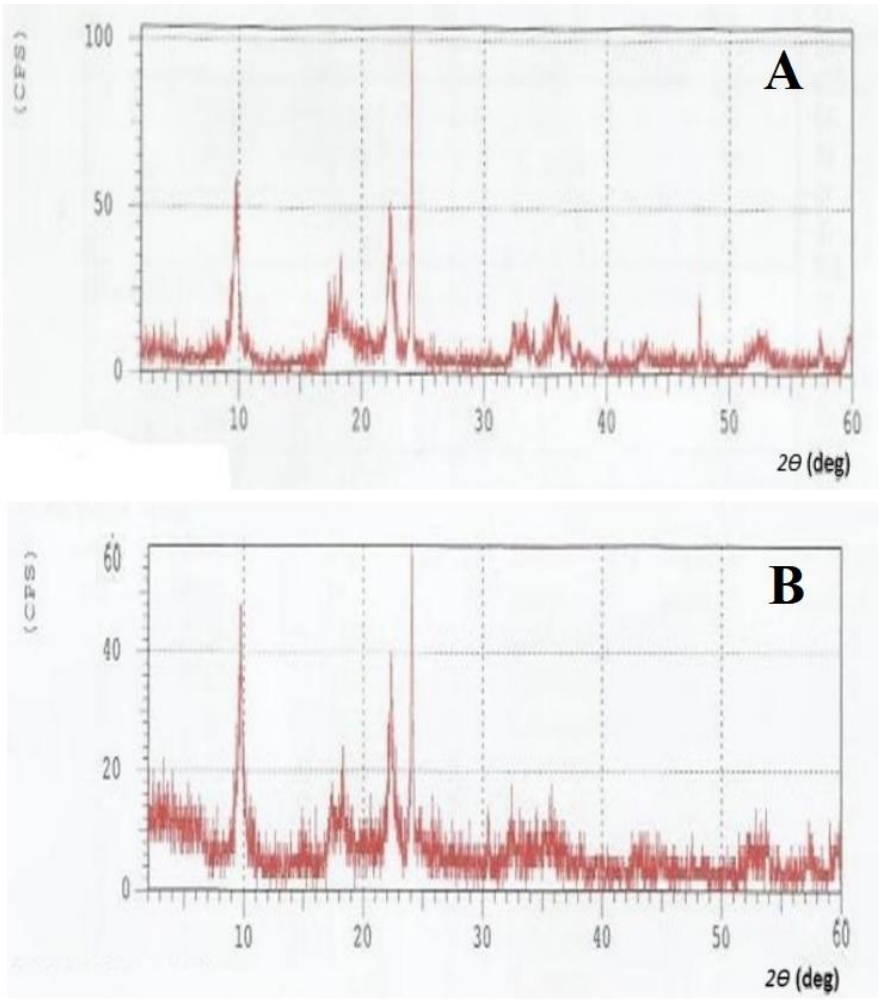


**Fig. 5. XRD pattern for (a) CB (b) CBC**

### 3.3.2 SEM image analyses

Figs. 4 (a) and (b) represents the scanning electron micrograph of CB and CBC, respectively. The SEM image of CB reveals the appearance of irregular platelet. This suggests that CB possesses rough edges, with crispy properties; a unique feature of animal tissues with high calcium content. Similarly, comparison of Fig 4 (b) and Fig 4 (a) shows characteristic improvement in the morphological features. Some of these improvements such as the formation of better cohesion, reduced individual lamella and the presence of a highly porous dark field matrix could be a direct consequence of HPA extraction process. This improved porous property is important for enhanced particle sticking required for surface phenomenon driven matrices like coagulation.

### 3.3.3 XRD analyses

The polymorphic features of a compound with different crystalline structures are determined using x-ray diffraction technique. The XRD pattern of CB and CBC are depicted in Figs. 5 (a) & (b), respectively. The XRD pattern of CB depicts a well organized spectral pattern with strong reflections $2\Theta$ values at 8 – 10, 17 – 19, 23 – 35 and 33 – $37^0$. While the XRD pattern of CBC shows similar reflections as those of CB at $2\Theta$ values but with low intensity peaks. The unorganized nature of the CBC spectral pattern and its low intensity values indicates that the CBC is a less crystalline poly-morph when compared to CB.

## 3.4 RSM Modelling

The combined effects of effluent pH, coagulant dosage, initial concentration, coagulation temperature and settling time on effluent turbidity reduction was studied using central composite design. The five-input experimental (consisting of 16 factorial points, 10 axial and 6 centre points) as well as the predicted values of percentage turbidity removal are presented in **Table 4**. Also, **Table 5** shows the relevant parameters generated from the analysis of variance (ANOVA). It should be noted that ANOVA technique employs the p-value and F-value to determine the adequacy and fitness of the empirical model. Hence, by comparing the model and lack of fit parameters, an F-value of 189.043 and a low p-value of 0.0001 as shown in **Table 5** implies that the model is significant. The model p-value of 0.0001 indicates that there is only 0.01% chance that the model F-value could occur due to noise. The values of "prob > F" less than 0.0500 indicate that model terms are significant.

Consequently, $x_1, x_2, x_3, x_5, x_1x_3, x_1x_4, x_1x_5, x_2x_4, x_2x_5, x_3x_4, x_3x_5, x_1^2, x_2^2 and x_5^2$ are significant model terms. The lack of fit f-value of 0.91 implies the lack of fit is not significant relative to pure error, and there is 58.59% chance that a lack of fit f-value this large could occur due to noise. This value of lack of fit implies that the model is well fitted (Ohale et al., 2022a). The smaller the magnitude of p-value, the greater the significance of the corresponding model term. From **Table 5**, effluent pH and coagulation temperature have the highest and the least influence respectively, on the final turbidity of the effluent, which is in agreement with the findings of other researchers [9, 11]. The predicted R-squared of 0.9675 is in reasonable agreement with the adjusted R-squared of 0.9765 because they are < 0.2 apart (Ohale et al., 2022a).

**Table 4. The CCD matrix along with the experimental and predicted values**

| Std order | Point type | pH | Dosage (g) | Initial Conc. (mg/L) | Temp. (K) | time (min) | EXP | RSM | ANN |
|---|---|---|---|---|---|---|---|---|---|
| 1 | Factorial | -1 | -1 | -1 | -1 | 1 | 197.9 | 201.1 | 197.9 |
| 2 | Factorial | 1 | -1 | -1 | -1 | -1 | 19.3 | 23.6 | 19.3 |
| 3 | Factorial | -1 | 1 | -1 | -1 | -1 | 167.9 | 171.1 | 167.9 |
| 4 | Factorial | 1 | 1 | -1 | -1 | 1 | 64.1 | 66.4 | 63.3 |
| 5 | Factorial | -1 | -1 | 1 | -1 | -1 | 294.7 | 300.7 | 294.7 |
| 6 | Factorial | 1 | -1 | 1 | -1 | 1 | 88.8 | 84.0 | 88.8 |
| 7 | Factorial | -1 | 1 | 1 | -1 | 1 | 117.1 | 113.2 | 118.7 |
| 8 | Factorial | 1 | 1 | 1 | -1 | -1 | 101.1 | 108.4 | 101.1 |
| 9 | Factorial | -1 | -1 | -1 | 1 | -1 | 30.8 | 32.3 | 30.8 |
| 10 | Factorial | 1 | -1 | -1 | 1 | 1 | 82.3 | 81.8 | 81.9 |

| Std order | Point type | pH | Dosage (g) | Initial Conc. (mg/L) | Temp. (K) | time (min) | EXP | RSM | ANN |
|---|---|---|---|---|---|---|---|---|---|
| 11 | Factorial | -1 | 1 | -1 | 1 | 1 | 137.0 | 135.3 | 137.0 |
| 12 | Factorial | 1 | 1 | -1 | 1 | -1 | 111.5 | 112.2 | 111.5 |
| 13 | Factorial | -1 | -1 | 1 | 1 | 1 | 156.6 | 157.8 | 156.6 |
| 14 | Factorial | 1 | -1 | 1 | 1 | -1 | 61.0 | 54.5 | 61.0 |
| 15 | Factorial | -1 | 1 | 1 | 1 | -1 | 424.1 | 418.5 | 424.1 |
| 16 | Factorial | 1 | 1 | 1 | 1 | 1 | 100.9 | 103.3 | 101.7 |
| 17 | Axial | -1.5 | 0 | 0 | 0 | 0 | 285.3 | 283.6 | 285.3 |
| 18 | Axial | 1.5 | 0 | 0 | 0 | 0 | 118.1 | 115.7 | 118.1 |
| 19 | Axial | 0 | -1.5 | 0 | 0 | 0 | 122.0 | 120.2 | 122.0 |
| 20 | Axial | 0 | 1.5 | 0 | 0 | 0 | 177.2 | 175.0 | 177.2 |
| 21 | Axial | 0 | 0 | -1.5 | 0 | 0 | 47.8 | 48.9 | 47.8 |
| 22 | Axial | 0 | 0 | 1.5 | 0 | 0 | 144.0 | 155.5 | 144.0 |
| 23 | Axial | 0 | 0 | 0 | -1.5 | 0 | 118.6 | 100.2 | 118.6 |
| 24 | Axial | 0 | 0 | 0 | 1.5 | 0 | 106.2 | 105.3 | 106.2 |
| 25 | Axial | 0 | 0 | 0 | 0 | -1.5 | 66.5 | 60.3 | 66.5 |
| 26 | Axial | 0 | 0 | 0 | 0 | 1.5 | 5.9 | 8.1 | 5.9 |
| 27 | Center | 0 | 0 | 0 | 0 | 0 | 102.1 | 102.7 | 102.6 |
| 28 | Center | 0 | 0 | 0 | 0 | 0 | 95.8 | 102.7 | 102.6 |
| 29 | Center | 0 | 0 | 0 | 0 | 0 | 116.8 | 102.7 | 102.6 |
| 30 | Center | 0 | 0 | 0 | 0 | 0 | 93.1 | 102.7 | 102.6 |
| 31 | Center | 0 | 0 | 0 | 0 | 0 | 104.6 | 102.7 | 102.6 |
| 32 | Center | 0 | 0 | 0 | 0 | 0 | 94.1 | 102.7 | 102.6 |

**Table 5. Analysis of variance table**

| Source | Sum of squares | dF | Mean square | F – value | p-value | |
|---|---|---|---|---|---|---|
| Model | 214254.700 | 15 | 14283.647 | 189.043 | < 0.0001 | Significant |
| $x_1$ | 64261.909 | 1 | 64261.909 | 850.502 | < 0.0001 | |
| $x_2$ | 6852.238 | 1 | 6852.238 | 90.689 | < 0.0001 | |
| $x_3$ | 22364.783 | 1 | 22364.783 | 295.996 | < 0.0001 | |
| $x_4$ | 59.070 | 1 | 59.070 | 0.782 | 0.3897 | |
| $x_5$ | 6205.656 | 1 | 6205.656 | 82.131 | < 0.0001 | |
| $x_1x_3$ | 9225.041 | 1 | 9225.041 | 122.093 | < 0.0001 | |
| $x_1x_4$ | 778.620 | 1 | 778.620 | 10.305 | 0.0055 | |
| $x_1x_5$ | 7744.497 | 1 | 7744.497 | 102.498 | < 0.0001 | |
| $x_2x_4$ | 21981.617 | 1 | 21981.617 | 290.925 | < 0.0001 | |
| $x_2x_5$ | 15970.407 | 1 | 15970.407 | 211.367 | < 0.0001 | |
| $x_3x_4$ | 3257.661 | 1 | 3257.661 | 43.115 | < 0.0001 | |
| $x_3x_5$ | 20251.712 | 1 | 20251.712 | 268.030 | < 0.0001 | |
| $x_1^2$ | 22189.884 | 1 | 22189.884 | 293.682 | < 0.0001 | |
| $x_2^2$ | 4751.627 | 1 | 4751.627 | 62.887 | < 0.0001 | |
| $x_5^2$ | 11103.631 | 1 | 11103.631 | 146.956 | < 0.0001 | |
| Residual | 1208.922 | 16 | 75.558 | | | |
| Lack of Fit | 806.794 | 11 | 73.345 | 0.912 | 0.5849 | not significant |
| Std. Dev. | 8.69 | | R-Squared | 0.9944 | | |
| Mean | 123.54 | | Adj R-Squared | 0.9891 | | |
| C.V. % | 7.04 | | Pred R-Squared | 0.9765 | | |

The final equation in terms of the coded factors is expressed as Eq. 9;

$$Finalturbidity = 102.73 - 55.99x_1 + 18.28x_2 + 35.88x_3 + 1.70x_4 - 17.40x_5 - 26.68x_1 + 6.9x_1x_4 + 22.0x_1x_5 + 37.07x_2x_4 - 31.59x_2x_5 + 15.85x_3x_4 - 39.53x_3x_5 + 43.08x_1^2 + 19.94x_2^2 - 30.48x_3^2 \quad (9)$$

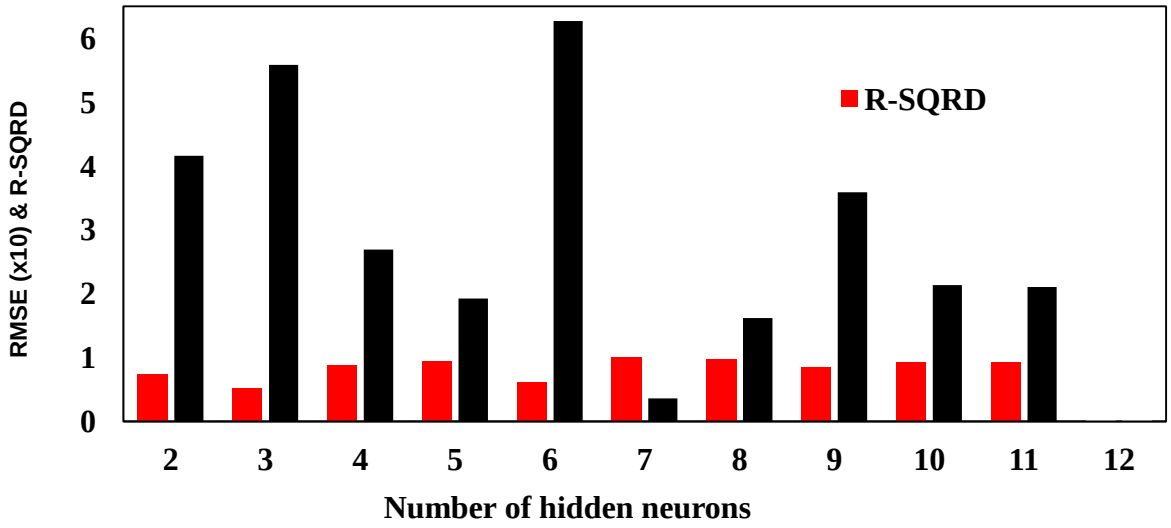


**Fig. 6. Effect of the neuron numbers in the hidden layer on the performance of the neural network**

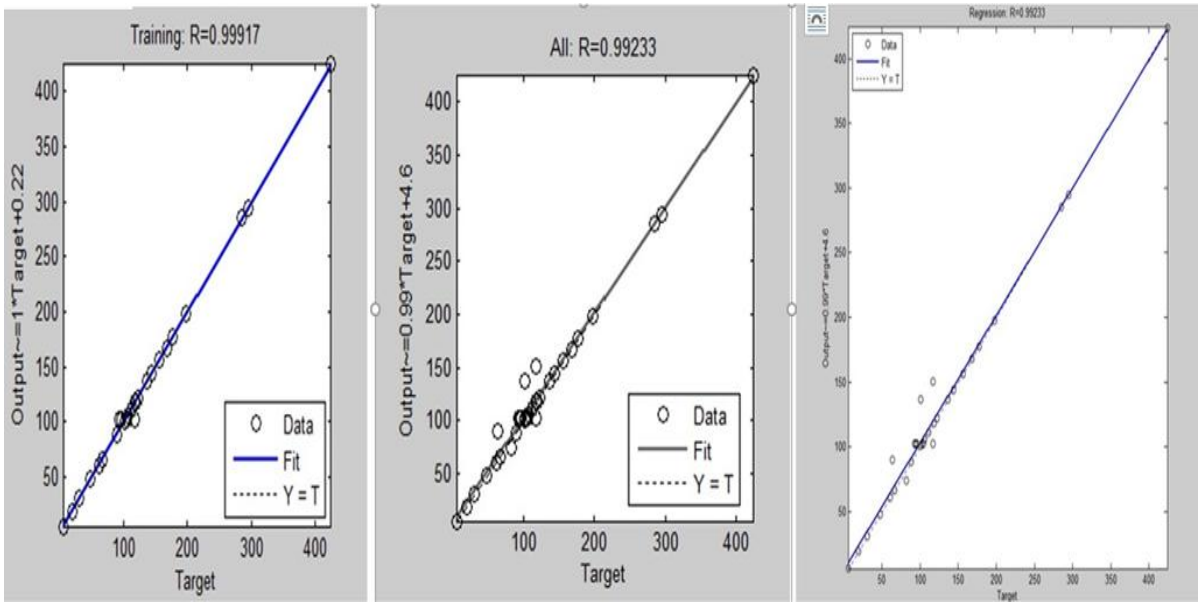


**Fig. 7. Regression analysis for ANN predicted values versus exp. (target) values**

## 3.5 ANN Modelling

Data set employed in ANN modeling was identical to those used in design of experiment (see Table 5). The graphical expression for the topological analysis is displayed in Fig. 6. Data partitioning as training set and test set were conducted to eliminate the issue of over-training and over parametrization. The 7 selected hidden neuron numbers produced the highest correlation coefficient (0.988) and the least root mean square error (RMSE) value (0.3701). Also, the regression plot (Fig. 7) showed a relatively high correlation coefficient ($R^2$> 0.95); thus suggesting a good correlation between the experimental and ANN predicted values.

## 3.6 Combined Effect of Operating Parameters on Final Turbidity

The contour plot in Figs. 8 – 11 shows the result for the combined effects of various process variables on the abattoir effluent final turbidity. The reduced effluent final turbidity (80.3 mg/L) observed in Fig. 8 was occasioned by an

increased coagulant dose (from 1.0 g/L to 1.3 g/L) at a constant pH. Further increase in coagulant dosage (beyond 1.3 g/L) impacted the final effluent turbidity negatively, as the removal efficiency of suspended particles decreased significantly (see Fig. 11). The observed decrease in final turbidity with increase in the coagulant dose (up to 1.3 g/L) could be due to the availability of more active sites necessary for coagulation process. According to Menkiti and Ejimofor [12], re-turbidization is caused by charge reversal due to over concentration of positively charged coagulant particles. This explains the reduction in turbidity removal efficiency (re-turbidization) when the coagulant dose is augmented beyond 1.3 g/L.

The combined effect of effluent pH and initial concentration is shown in Fig. 9. It could be observed that the coagulant displayed maximum turbidity reduction (58.6 mg/L) at neutral environment (pH 6.7) and at constant effluent initial concentration of 183.0 mg/L. Such observation could be explained by the fact that the buffer nature of the effluent tends to enhance the precipitation of the coagulant around neutral pH$(6.5 \leq pH \leq 7.0)$. However, the adjustment of the effluent pH either to the acidic or alkaline region was met with a significant reduction in turbidity removal efficiency $(final\ turbidity < 50.0\ mg/L)$. This is due to the disappearance of the effluent buffer nature at pH values outside the neutral environment; thus resulting in coagulant precipitation difficulties. The effect of initial effluent concentration shows that low initial concentration of raw effluent results in a low final turbidity. However, an increment in the effluent initial concentration results in low removal efficiency and a high final turbidity value. This phenomenon could be attributed to lack of sufficient active site for the removal of turbid particles at high concentration.

The effect of coagulation temperature and settling time is shown in the 2-D contour plot of Fig. 10. It could be observed that at high temperature, an accelerated settling rate was recorded; thus resulting in low final turbidity of the treated effluent. This observation could be explained by the fact that temperature increase bears positive effect on coagulation and flocculation process by altering the solubility and also reduces the effluent viscosity, thereby allowing for higher dispersion of CBC particles which aided floc formation and cell enmeshment (Ohale et al., 2020).

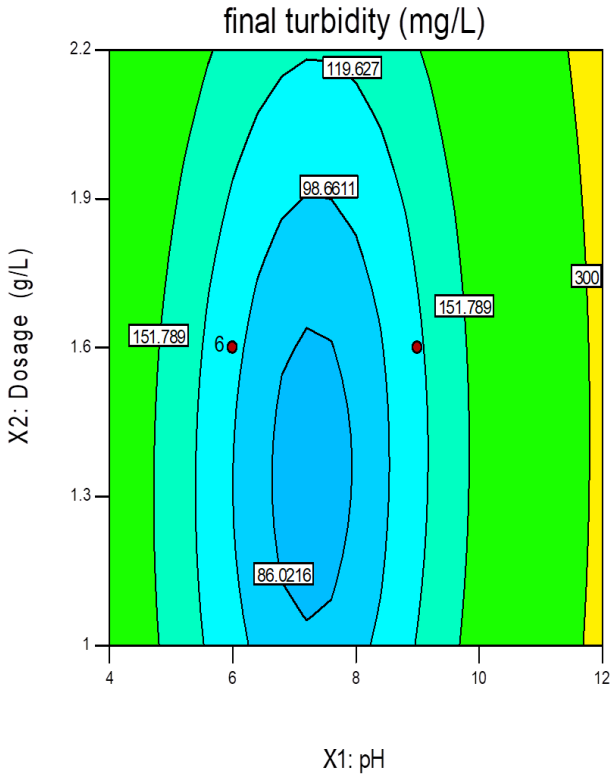


**Fig. 8. 2D contour for the combined effects of coagulant dosage and effluent pH**

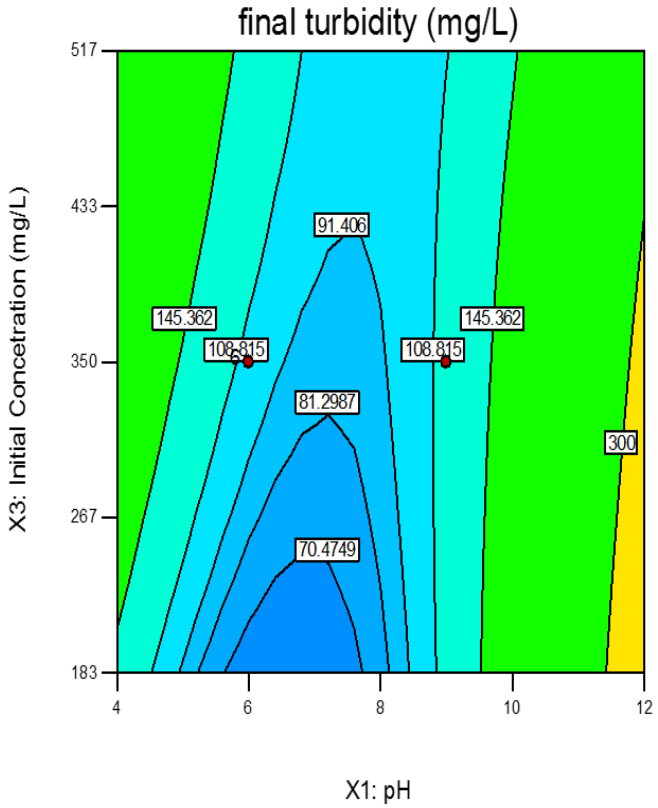


**Fig. 9. 2D contour for the combined effects of effluent initial concentration and effluent pH**

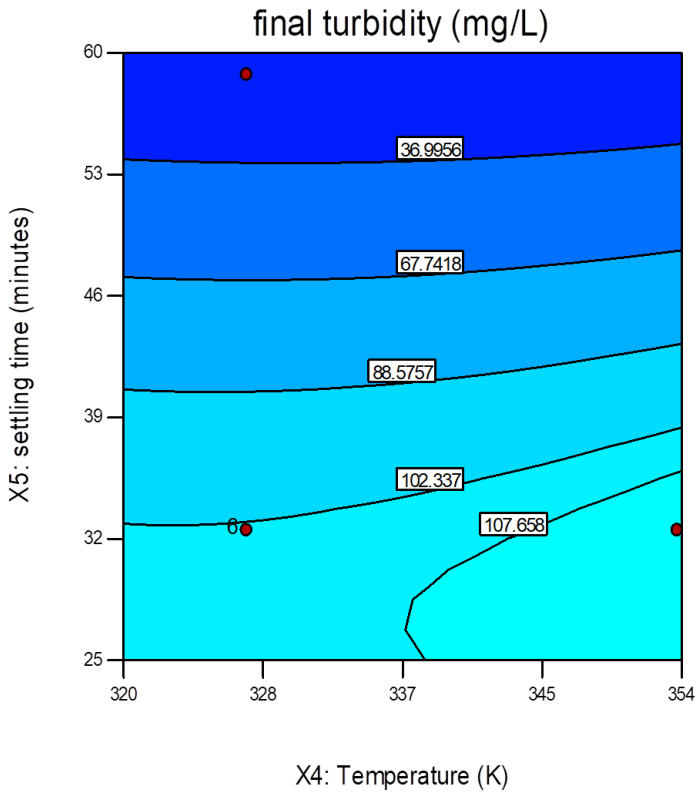


**Fig. 10. 2D contour for the combined effects of settling time and coagulation temperature**

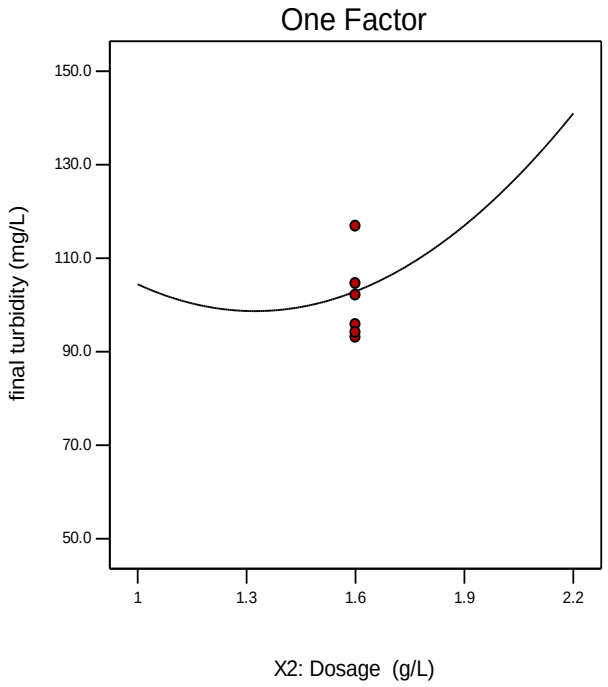


**Fig. 11.Effect of coagulant dosage on the final turbidity.**

### 3.7 ANN and RSM Comparative Analyses

In order to ascertain the superiority of either of the optimization tools (ANN and RSM) over the other in predicting the non-linear behavior of the present system, error functions were employed. The coefficient of determination ($R^2$), mean square error (MSE), and absolute average relative deviation (AARD) were the error functions used to compare the predictions accuracy of both models. MSE and AARD values were evaluated from Eqs.10 & 11, respectively; while the coefficient of determination ($R^2$) values was estimated from Fig. 12. From the values of $R^2$, MSE and AARD shown in Table 6, the ANN predictions produced a higher regression coefficient and a negligible deviation from experimental values when compared to the RSM predictions. This confirms that ANN technique as against RSM technique portrayed better accuracy in capturing the non-linear nature of the coagulation process.

$$MSE = \frac{1}{n}\sum_{i=1}^{n}\left(y_{i,}predic. - y_{i,}\exp.\right)^2 \qquad (10)$$

$$AARD(\%) = \frac{1}{n}\sum_{i=1}^{n}\left(\left|\frac{\left(y_{i,}predic. - y_{i,}\exp.\right)}{\left(y_{i,}\exp.\right)}\right|\right)\times 100 \qquad (11)$$

Where; $y_{i,predic.}$ , $y_{i,\exp.}$ and $n$ are final turbidity obtained by the predicted model, the experimental data and the number of experimental data, respectively.

Fig. 13 shows the comparative parity plot for the RSM, ANN models and the experimental data versus experimental run number. High correlation could be observed between the ANN and experimental data points. Meanwhile, in comparison with the experimental data point, the RSM data point showed significant deviations especially at run numbers 14, 22 and 23; with magnitudes of 5.6, 11.4 and 18.4, respectively. The correlation depicted by ANN data points in relation to the experimental values further gave credence to the superiority of ANN model over the RSM model with respect to the present study.

### 3.8 Optimization using ANN-Genetic Algorithm (ANN-GA) Technique

The objective of process optimization is to search for the optimum process conditions to establish the minimum final turbidity. In this approach, the ANN-GA was used to generate the model values. Eqs. 12 – 16 show the selected range of constraints for each variable. Also, the technique of hybrid ANN-GA algorithm used in this work is illustrated in Fig. 14.

$$6.5 \le pH \le 7.5 \quad (12)$$

$$1.0g/L \le dosage \le 1.5g/L \quad (13)$$

$$183mg/L \le initialconc. \le 250mg/L \quad (14)$$

$$310K \le Temp. \le 345K \quad (15)$$

$$30\min. \le settlingtime \le 50\min. \quad (16)$$

However, based on afore mention evaluation an optimal final turbidity of 4.96 mg/L was obtained pH = 6.7, dosage = 1.003 g/L, initial conc. = 182.2 mg/L, coagulation temperature = 345 K and settling time = 36 min. Duplicate validation experiments were conducted in order to uphold the optimal predicted value. Using the optimum variable conditions, the average final turbidity obtained was 5.53 ± 0.24 (mg/L). The treated effluent obtained after the validation experiment was characterized and the results are shown on Table 7. The characterization result shows that the model prediction was in agreement with the experimental value.

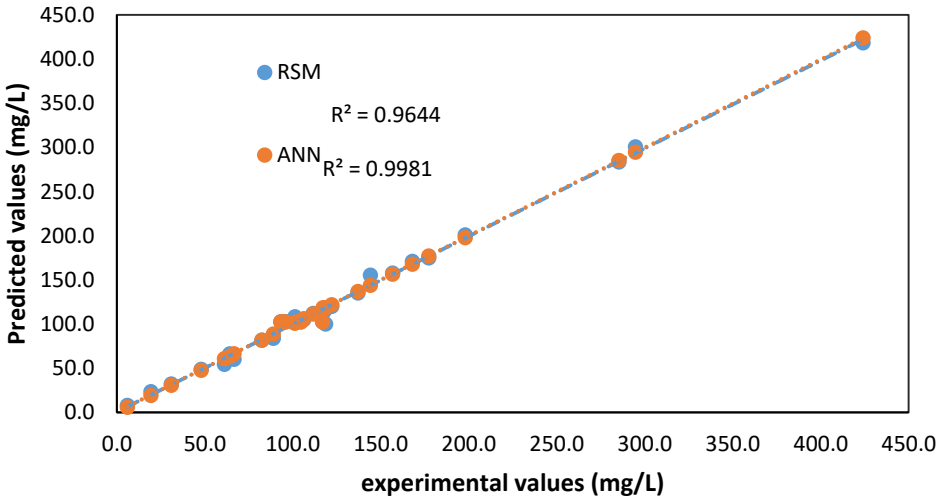


**Fig. 12. RSM and ANN model appraisal**

**Table 6. Comparison of predictive competency of RSM and ANN**

| | RSM | ANN |
|---|---|---|
| MSE | 37.78 | 13.11 |
| $R^2$ | 0.9644 | 0.9981 |
| AARD | 5.93 | 1.43 |

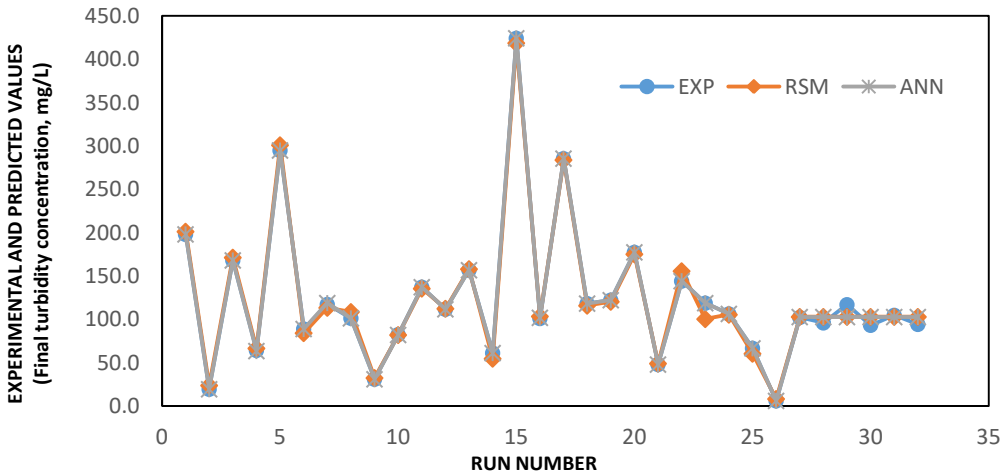


**Fig. 13. A plot depicting the comparison between the experimental and predicted values for the ANN and RSM models**

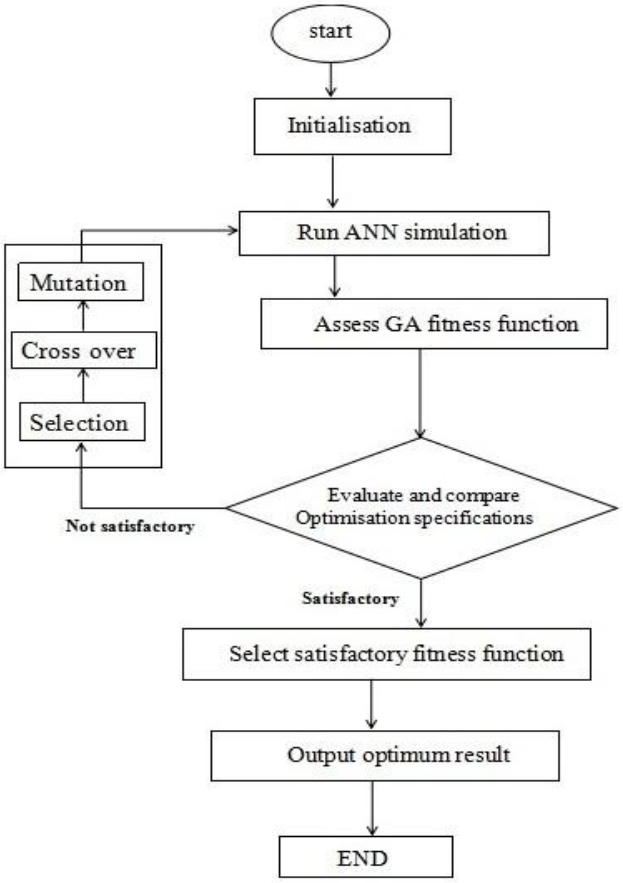


**Fig. 14. Flow chart of combining ANN-GA optimisation technique**

**Table 7. Post optimal characterization results of the abattoir waste water**

| Parameter | Treated abattoir |
|---|---|
| Final turbidity concentration (mg/L) | 5.3 |
| Total suspended solids (mg/L) | 2.5 |
| Total solids (mg/L) | 3.1 |
| Biological oxygen demand (mg/L) | 8.6 |
| Chemical oxygen demand (mg/L) | 152 |
| pH | 8.1 |
| Odour | Slightly alkaline |
| Colour | Clear colourless |

## 4. CONCLUSION

In this work, the coag-flocculation of abattoir waste water was studied using HPA derived from raw CB. RSM and ANN modelling techniques were comparatively used in predicting the final turbidity of the effluent. Statistical techniques ($R^2$ and RMSE) were employed in selecting the most appropriate hidden number of neurons. Multi-layer neural network (5-7-1) was chosen to develop accurate and complex nonlinear relationship. From the results of the comparative analysis, ANN model was found to perform better in capturing the non-linear nature of the system. Process optimization using ANN-GA technique gave an optimum value of 4.92 mg/L for final effluent turbidity at pH = 6.7, dosage = 1.003 g/L, initial conc. = 182.2 mg/L, coagulation temperature = 345K and settling time = 36 min. This value was validated by a set of duplicate experiments producing an average value of 5.53 ± 0.24 (mg/L) which is in close agreement with the predicted value.

## FUNDING

This research work was supported by the Tertiary Education Trust Fund, Nigeria through Institution Based Research grant (IBR). Years: TETFUND Research Projects (RP) Intervention Funds, (2016-2017 merged intervention). Ref: TETFUND/DESS/UNI/AWKA/2017/RP/VOL.1

## COMPETING INTERESTS

Authors have declared that no competing interests exist.

## REFERENCES

1. Emembolu LN, Nwabanne JT, Onu CE. Kinetic modeling of anaerobic digestion of restaurant waste water. British Journal of Applied Science & Technology. 2017;21(4):1-12. Available:https://doi.org/10.9734/BJAST/2017/33397
2. Mshelbwala GM. National livestock policy focal point presentation –Nigeria. Paper presented at Side-meeting of NLPFPS on VET-GOV programme engagement / targetting and capacity building facilitation Abidjan, Cote D'ivoire; 2013.
3. Ogbeide OA. Meat industry development in Nigeria: implications of the consumers' perspective. Mayfair Journal of Agribusiness Management. 2015;1:59- 75.
4. Ohale PE, Onu CE, Nwabanne JT, Aniagor CO, Okey-Onyesolu CF, Ohale NJ. A comparative optimization and modeling of ammonia–nitrogen dsorption from abattoir wastewater using a novel iron-functionalized crab shell. Applied Water Science. 2022;12(193):1-27. Available:https://doi.org/10.1007/s13201-022-01713-4
5. Obi CC, Nwabanne JT, Igwegbe CA, Ohale PE, Okpala CO. Multi characteristic optimization and modeling analysis of electrocoagulation treatment of abattoir wastewater using iron electrode pairs. Journal of Water Process Engineering. 2022;49:103136. Available:https://doi.org/10.1016/j.jwpe.2022.103136
6. Nwabanne JT, Iheanacho OC, Obi CC et al. Linear and nonlinear kinetics analysis and adsorption characteristics of packed bed column for phenol removal using rice husk-activated carbon. Appl Water Sci. 2022;12:91. Available:https://doi.org/10.1007/s13201-022-01635-1
7. Kundu P, Debsarkar A, Mukherjee S. Treatment of slaughter house wastewater in a sequencing batch reactor: performance evaluation and biodegradation kinetics. Hindawi Publishing Corporation BioMed Research International. 2013;11(1):15. Available:https://doi.org/10.1155/2013/134872
8. Bazrafshan E, Zakeri HR, Vieira MGA, Derakhshan Z, Mohammadi L, Mohammadpour A, Mousavi Khaneghah A. Slaughterhouse wastewater treatment by integrated chemical coagulation and electro-fenton processes. Sustainability. 2022;14:11407. Available:https://doi.org/10.3390/su141811407
9. Menkiti MC, Sekaran G, Ugonabo VI, Menkiti UN, Onukwuli OD. Factorial optimisation and kinetic studies of coagulation-flocculation of brewery effluent by crab shell coagulant. Journal of Chinese Advanced Materials Society. 2015;4:36 – 61. Available:https://doi.org/10.1080/22243682.2015.1048287
10. Okan OL, Ugonabor VI, Onu CE, Chinedu JU. Application of trickling filter with hybrid biofilm support media in the treatment of petroleum effluent. LAUTECH Journal of Engineering and Technology. 2022;16 (2):94-105.
11. Ohale PE, Onu CE, Ohale NJ, Oba SN. Adsorptive kinetics, isotherm and thermodynamic analysis of fishpond effluent coagulation using chitin derived coagulant from waste Brachyura shell. Chemical Engineering Journal Advances. 2020;4:100036. Available:https://doi.org/10.1016/j.ceja.2020.100036
12. Menkiti MC, Ejimofor M. Experimental and artificial neural network application on the optimization of paint effluent (PE) coagulation using novel acatinodea shell extract (ASE). JWPE; 2016;10:172-187. Available:https://doi.org/10.1016/j.jwpe.2015.09.010
13. Al-Mutairi NZ, Hamoda MF, Al-Ghusain I. Coagulant selection and sludge conditioning in a slaughterhouse wastewater treatment plant. Bioresource Technology. 2004;95:115–119.

14. Available:https://doi.org/10.1016/j.biortech.2004.02.017
15. Amuda OS, Alade A. Coagulation/flocculation process in the treatment of abattoir wastewater. Desalination. 2006;196:22–31. Available:https://doi.org/10.1016/j.desal.2005.10.039
16. Aquilar MI, Sáez J, Llorens SM, Ortuño JF, Meseguer V, Fuentes A. Improvement of coagulation-flocculation process using anionic polyacrylamide as oagulant aid. Chemosphere. 2005;58L47–56. Available:https://doi.org/10.1016/j.chemosphere.2004.09.008
17. Mahtaba A, Tariq M, Shafiq T, Nasir A. Coagulation/adsorption combined treatment of slaughterhouse wastewater. Desalination and Water Treatment. 2009;12:270-275. Available:https://doi.org/10.5004/dwt.2009.952
18. Katayon S, Megat-Mohd MJ, Asma M, Abdul-Ghani LA, Thamer AM, Azni I, Ahmad J, Khor BC, Suleyman AM. Effects of storage conditions of *Moringa oleifera* seeds on its performance in coagulation. Bioresource Technology. 2006;97:1455–60. Available:https://doi.org/10.1016/j.biortech.2005.07.031
19. Ghedjemis A, Riad Ayeche R, Maya Kebaili M, Ali Benouadah A, Laurent Frédéric Gil L. Application of natural hydroxyapatite in the treatment of polluted water: Utilization of dromedary bone as bioadsorbent, International of applied ceramic technology; 2022. Available:https://doi.org/10.1111/ijac.14041
20. Choumane FZ, Benguella B, Maachou B, Saadi N. Valorisation of a bioflocculant and hydroxyapatites as coagulation-flocculation adjuvants in wastewater treatment of the steppe in the wilaya of Saida (Algeria), Ecological Engineering. 2017;107:152–159. Available:http://dx.doi.org/10.1016/j.ecoleng.2017.07.013
21. Brazdis RI, Fierascu I, Avramescu SM, Fierascu RC. Recent progress in the application of hydroxyapatite for the adsorption of heavy metals from water matrices. Materials. 2021;14:6898. Available:https://doi.org/10.3390/ma14226898
22. Marrane SE, Dänoun K, Allouss D, Sair S, Channab B, Rhihil A, Zahouily M. A novel approach to prepare cellulose‑g‑hydroxyapatite originated from natural sources as an efficient adsorbent for heavy metals: batch adsorption optimization via response surface methodology. ACS Omega. 2022;7:28076−28092. Available:https://doi.org/10.1021/acsomega.2c02108
23. Onu CE, Igbokwe PK, Nwabanne JT, Ohale PE. ANFIS, ANN, and RSM modeling of moisture content reduction of cocoyam slices. Journal of Food Processing and Preservation. 2022a;46:10. Available:https://doi.org/10.1111/jfpp.16032
24. Ohale PE, Uzoh CF, Onukwuli OD. Optimal factor evaluation for the dissolution of alumina from Azaraegbelu clay in acid solution using RSM and ANN comparative analysis, South African Journal of Chemical Engineering. 2017;24:43 – 54. Available:https://doi.org/10.1016/j.sajce.2017.06.003
25. Nwadike EC, Abonyi MN, Nwabanne JT, Ohale PE. Optimization of solar drying of blanched and unblanched aerial yam using response surface methodology. International Journal of Trend in Scientific Research and Development. 2020;4(3):659 – 666.
26. Onu et al. Modeling, optimization, and adsorptive studies of bromocresol green dye removal using acid functionalized corn cob. Cleaner Chemical Engineering. 2022b;4:00067. Available:https://doi.org/10.1016/j.clce.2022.100067
27. Nwobasi VN, Igbokwe PK, Onu CE. Optimization of acid activated ngbo clay catalysts in esterification reaction using response surface methodology. Asian Journal of Physical and Chemical Sciences. 2022;10(1):11-27. Available:https://doi.org/10.9734/AJOPACS/2022/v10i130147
28. Onu CE, Nwabanne JT, Ohale PE, Asadu CO. Comparative analysis of RSM, ANN and ANFIS and the mechanistic modeling in eriochrome black-T dye adsorption using modified clay. South African

Journal of Chemical Engineering. 2021;36: 24–42.
Available:https://doi.org/10.1016/j.sajce.2020.12.003

29. Onu CE, Nwabanne JT. Application of response surface methodology in malachite green adsorption using nteje clay. Open Journal of Chemical Engineering and Science. 2014;1(2):19 - 33.
30. Onu CE, Igbokwe KP, Nwabanne JT, Charles OC, Ohale PE. Evaluation of optimization techniques in predicting optimum moisture content reduction in drying potato slices. Artificial Intelligence in Agriculture. 2020;4:39–47.
Available:https://doi.org/10.1016/j.aiia.2020.04.001
31. Emembolu LN, Ohale PE, Onu CE, Ohale NJ. Comparison of RSM and ANFIS modeling techniques in corrosion inhibition studies of Aspilia Africana leaf extract on mild steel and aluminium metal in acidic medium. Applied Surface Science Advances. 2022;11: 100316.
Available:https://doi.org/10.1016/j.apsadv.2022.100316
32. Jamil S, Zhonghua S, Mingshan J, Zumin G, Waqas A. ANN and RSM based modeling for optimization of cell dry mass of Bacillus sp. strain B67 and its antifungal activity against botrytis cinerea, Biotechnol. Biotechnol. Equip. 2018;32(1): 58-68.
Available:https://doi.org/10.1080/13102818.2017.1379359
33. Onu CE,Nweke CN, Nwabanne JT. Modeling of thermo-chemical pretreatment of yam peel substrate for biogas energy production: RSM, ANN, and ANFIS comparative approach. Applied Surface Science Advances. 2022c;11:100299.
Available:https://doi.org/10.1016/j.apsadv.2022.100299
34. Pakravan P, Akhbari A, Moradi H, Azandaryani AH, Mansouri AM, Safari M. Process modeling and evaluation of petroleum refinery wastewater treatment through response surface methodology and artificial neural network in a photocatalytic reactor using poly ethyleneimine (PEI)/titania (TiO2) multilayerfilm on quartz tube. Appl Petrochem Res. 2015;5:47–59.
Available:https://doi.org/10.1007/s13203-014-0077-7
35. Sodeifian G, Sajadian SA, Ardestani NS. Evaluation of the response surface and hybrid artificial neural network genetic algorithm methodologies to determine extraction yield of Ferulago angulata through super critical fluid. Journal of the Taiwan Institute of Chemical Engineers. 2016;60:165–173.
Available:https://doi.org/10.1016/j.jtice.2015.11.003
36. Brzezińska-Miecznikn J, Haberko K, Sitarz M, Bućko MM, Macherzyńska B. Hydroxyapatite from animal bones – Extraction and properties, Ceramics international; 2015.
Available:http://dx.doi.org/10.1016/j.ceramint.2014.12.041
37. Clesceri LS, Greenberg AE, Eaton AD. Standard methods for the examination of water and wastewater, american public health association, america water works association, water environment federation, Washington, DC,USA, 29th edition; 1998.
38. Ohale PE, Nwajiobi OJ, Onu CE, Madiebo EM, Ohale NJ. Solvent extraction of oil from three cultivars of Nigerian mango seed kernel: Process modeling, GA - optimization, nonlinear kinetics and comparative characterization, Applied Food Research. 2022b;2(2):100227.
Available:https://doi.org/10.1016/j.afres.2022.100227
39. Coutts RT. In: Chatten,L. G., (ed). Pharmaceutical chemistry – instrumental techniques. CBS Publishers and Distributors PVT Ltd., New Delhi, India. 2008;59–125.



*Peer-review history:*
*The peer review history for this paper can be accessed here:*
*https://www.sdiarticle5.com/review-history/94359*